

Fast evaluation of interaction integrals for confined systems with machine learning

A. Mreńca-Kolasińska, K. Kolasiński, and B. Szafran
*AGH University of Science and Technology,
Faculty of Physics and Applied Computer Science,
al. Mickiewicza 30, 30-059 Kraków, Poland*

The calculation of interaction integrals is a bottleneck for the treatment of many-body quantum systems due to its high numerical cost. We conduct configuration interaction calculations of the few-electron states confined in III-V semiconductor two-dimensional structures using a shallow neural network to calculate the two-electron integrals, which can be used for general isotropic interaction potentials. This approach allows for a speed-up of the evaluation of the energy levels and controllable accuracy.

I. INTRODUCTION

Computation of quantum problems for interacting particles is a challenging task that has been dealt with using various approaches, including machine learning (ML)^{1–13}. The difficulty of accurate many-body calculations arises from the high dimensionality of the space required when taking into account the electron-electron and electron-ion interactions. Methods developed to solve the many-body quantum problems include the density functional theory (DFT)¹⁴, Hartree-Fock method^{15,16}, and configuration interaction (CI) method^{17–20}. These methods contain the computation of the non local potentials due to the particle-particle interaction. This is a computationally demanding task because of its $\mathcal{O}(n_x^2)$ nature, with n_x being the mesh size. A number of approaches trying to improve the scalability of the non-local potential computation exist, with probably the most common being methods based on the Fourier transform which allow us to reduce the computational complexity to $\mathcal{O}(n_x \log(n_x))$.

The problem of the nonlocal potential calculation has been tackled using plane-wave functions and Gaussian-sum (GS) approximations^{21–23}. The authors of Ref. 22 developed a method of calculating the kernel via expansion of the density in terms of scaling functions and approximation of the $1/r$ potential in terms of Gaussian functions, which served to avoid the costly three-dimensional integral of the original kernel. Reference 23 proposed an approach to improve the accuracy based on the GS approximation of the kernel with a near-field correction added to account for the discrepancy between the GS-approximated and original kernels.

On the other hand, calculations for complex quantum systems were done using machine-learning methods. The problem was solved through the variational quantum Monte Carlo method^{8,9} or using ML for effective models¹⁰, which are also used in self-learning Monte Carlo methodologies^{11–13}.

In this work we propose an approach to solve the few-electron problem via the CI method. The need to calculate a huge number of Coulomb integrals^{24–26} is a main bottleneck of this method. Although the number of integrals can be reduced by taking into consideration sym-

metries of the problem and building a basis out of functions that satisfy some constraints (e.g., have the necessary spatial symmetry or spin), the calculation time of Coulomb integrals prevails in this problem, especially in two or more dimensions. The methods of the calculation of the nonlocal potential developed in Refs.^{21–23} mostly aim to obtain the best precision of the calculations. On the other hand, our objective is to develop an approximate and fast method which can be used to evaluate the energies of few-electron states with a precision sufficient to describe the quantum phenomena in mesoscopic systems.

In this paper we develop a method to calculate the two-electron integrals based on a shallow neural network²⁷ which can be used for any interaction potential that is isotropic. We present the application of our approach for Coulomb as well as non-Coulomb potentials in one or two dimensions. This method can be extended to three dimensions as well. The source code for the implementation of the proposed method is available online²⁸.

II. METHODS

A. Hamiltonian

We consider N electrons confined in a one- or two-dimensional III-V semiconductor nanostructure. The Hamiltonian, within the effective-mass approximation, is

$$H = \sum_{i=1}^N h_i + \sum_{i=1}^N \sum_{j>i}^N u(\mathbf{r}_i - \mathbf{r}_j), \quad (1)$$

where $u(\mathbf{r}_i - \mathbf{r}_j)$ is the interaction potential between the i th and j th electron and h_i is the single-electron Hamiltonian

$$h_i = -\frac{\hbar^2}{2m^*} \nabla_i^2 + V(\mathbf{r}_i), \quad (2)$$

with $V(\mathbf{r}_i)$ being the external potential at position \mathbf{r}_i . The interaction potential may have various forms, depending on the dimensionality of the system. In thin insulating layers it gets an effective form different from the Coulomb interaction potential due to screening²⁹, and for

quasi-one-dimensional systems it has the form of the exponentially scaled complementary error function³⁰. We will focus on isotropic interaction potentials that satisfy $u(\mathbf{r}_i - \mathbf{r}_j) = u(|\mathbf{r}_i - \mathbf{r}_j|)$.

The calculation is performed using the CI method^{19,24,31} within the basis set formed by Slater determinants Φ_k constructed from the one-electron wave functions

$$\Psi_n(\mathbf{r}_1, \dots, \mathbf{r}_N) = \sum_k c_k^{(n)} \Phi_k(\mathbf{r}_1, \dots, \mathbf{r}_N) \quad (3)$$

$$\Phi_k(\mathbf{r}_1, \dots, \mathbf{r}_N) = \frac{1}{\sqrt{N!}} \begin{vmatrix} \phi_{k_1}(\mathbf{r}_1) & \dots & \phi_{k_N}(\mathbf{r}_1) \\ \vdots & \ddots & \vdots \\ \phi_{k_1}(\mathbf{r}_N) & \dots & \phi_{k_N}(\mathbf{r}_N) \end{vmatrix} \quad (4)$$

As the single-electron wave functions ϕ_k we use the eigenfunctions of the h operator in the first-order finite-difference approximation on a mesh of points. The coefficients $c_k^{(n)}$ are found by solving the eigenproblem of the matrix with the elements given by

$$H_{pq} = \langle \Phi_p | H | \Phi_q \rangle. \quad (5)$$

Using the Slater-Condon rules, one can show that the matrix elements H_{pq} can be represented in terms of the one-electron and two-electron integrals:

$$\begin{aligned} \langle i|h|j \rangle &= \int d\mathbf{r}_1 \phi_i^*(\mathbf{r}_1) h(\mathbf{r}_1) \phi_j(\mathbf{r}_1), \\ \langle ij|u(\mathbf{r}_1 - \mathbf{r}_2)|kl \rangle &= \int d\mathbf{r}_1 d\mathbf{r}_2 \phi_i^*(\mathbf{r}_1) \phi_j^*(\mathbf{r}_2) u(\mathbf{r}_1 - \mathbf{r}_2) \phi_l(\mathbf{r}_2) \phi_k(\mathbf{r}_1). \end{aligned}$$

We use a basis formed with Slater determinants built with a finite number of one-electron states ϕ_k . Their number is determined by verifying, by the convergence of the energies of an N -electron system and given a basis containing n states, we have $\binom{n}{N}$ Slater determinants.

B. Evaluation of the two-electron integrals

The two-electron integral can be written as

$$\langle ij|u(\mathbf{r}_1 - \mathbf{r}_2)|kl \rangle = \int d\mathbf{r}_1 \phi_i^*(\mathbf{r}_1) u_{jl}(\mathbf{r}_1) \phi_k(\mathbf{r}_1), \quad (6)$$

where the effective potential $u_{jl}(\mathbf{r}_1)$ is

$$u_{jl}(\mathbf{r}_1) = \int d\mathbf{r}_2 \phi_j^*(\mathbf{r}_2) u(\mathbf{r}_1 - \mathbf{r}_2) \phi_l(\mathbf{r}_2). \quad (7)$$

Denoting the complex function $\rho_{jl}(\mathbf{r}_2) = \phi_j^*(\mathbf{r}_2) \phi_l(\mathbf{r}_2)$, one can reformulate the integral as a convolution operation

$$u_{jl}(\mathbf{r}_1) = \int d\mathbf{r}_2 u(\mathbf{r}_1 - \mathbf{r}_2) \rho_{jl}(\mathbf{r}_2) = (u * \rho_{jl})(\mathbf{r}_1), \quad (8)$$

where the asterisk (*) is the convolution operator and $u(\mathbf{r})$ is a nonlocal kernel, e.g., Coulomb interaction $u(r) \approx 1/r$.

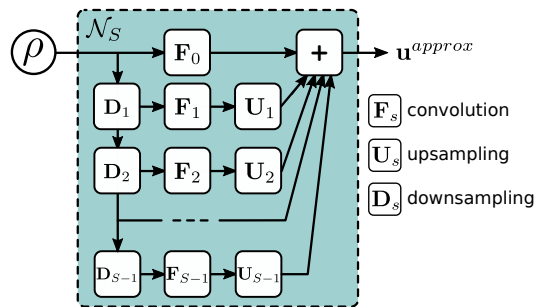


FIG. 1. Schematic of the neural net trained to evaluate the two-electron integrals described by Eq. (9).

1. Evaluating integrals with fast Fourier transform

The integral in Eq. (8) can be efficiently evaluated using the fast Fourier transform (FFT) method available in many numerical libraries³². For example, in the case of a one-dimensional grid of size n_x the computational cost of evaluating a single integral with FFT is

$$\mathcal{O}((n_x + P) \log(n_x + P)),$$

where P is a padding which is added to both sides of the grid symmetrically. The size of the padding depends on the size of the convolutional kernel. For closed systems (i.e., systems for which $\rho_{jl} = 0$ outside the computational box) with long-range interactions, the size of the kernel is $2n_x + 1$, and the size of the padding is equal to the size of the computational box $P = n_x$. We use this approach as our baseline method. However, in the special case of short-range interactions, the convolution kernel may be truncated, and $P \ll n_x$. In such a case padding has a negligible effect on the computation time. From the above we can see that the evaluation time of the integral in Eq. (8) can be improved in two ways, (a) truncating the kernel size, which will reduce padding, or (b) using faster implementation of FFT.

In this paper we show that the long-range interaction kernel can be approximated by a series of finite-size kernels for which $P \ll n_x$, so that the total computational time is smaller than the baseline FFT implementation. Additionally, we show that using the existing neural network frameworks^{33,34}, we can improve further the computational cost using efficient graphics processing unit (GPU) implementations of the convolution operator. The CPU implementation of the convolution is performed using the fast Fourier transform from the Intel[®] MKL library in the Fortran language and GPU implementation is provided in the Python language and TensorFlow framework.

2. Approximating the integral in one dimension

Let ρ be a discretized one-dimensional (1D) density array of size n_x . We define the downsampling operator

\mathbf{D}_s as

$$\hat{\boldsymbol{\rho}} = \mathbf{D}_s \boldsymbol{\rho},$$

which reduces the spatial size of $\boldsymbol{\rho}$ by a factor of 2 in the s th step (for example, starting from $s = 0$ with $n_x = 512$, operator \mathbf{D}_1 downsamples $\boldsymbol{\rho}$ to $n_x = 256$, \mathbf{D}_2 downsamples $\boldsymbol{\rho}$ from 256 to 128, and so on). In our implementation we use a standard average pool operator, defined as

$$\hat{\rho}_i = \frac{1}{2}(\rho_{2i} + \rho_{2i+1}), \quad i \in (1, n_x/2).$$

Similarly, we define the upsampling operator \mathbf{U}_s as

$$\hat{\boldsymbol{\rho}} = \mathbf{U}_s \boldsymbol{\rho},$$

which in the s th step resizes the input array back to size n_x (for example, for $s = 0$ it is an identity operation). In practice, the composition of the downsampling and upsampling operations results in an approximated identity operation

$$\mathbf{U}_s \mathbf{D}_s \mathbf{D}_{s-1} \dots \mathbf{D}_1 \boldsymbol{\rho} \approx \boldsymbol{\rho}.$$

For the upsampling operation we use the standard bilinear interpolation (e.g. `resize_bilinear` operator from the TensorFlow library³³). The role of the downsampling operation is to increase the receptive field.

We approximate the integral in Eq. (8) with the following definition of the linear neural network:

$$\begin{aligned} \mathbf{u}^{approx} &= \mathbf{F}_0 \boldsymbol{\rho} + \mathbf{U}_1 \mathbf{F}_1 \mathbf{D}_1 \boldsymbol{\rho} + \mathbf{U}_2 \mathbf{F}_2 \mathbf{D}_2 \mathbf{D}_1 \boldsymbol{\rho} \\ &+ \dots + \mathbf{U}_{S-1} \mathbf{F}_{S-1} \mathbf{D}_{S-1} \dots \mathbf{D}_2 \mathbf{D}_1 \boldsymbol{\rho} \quad (9) \\ &= \mathcal{N}_S(\boldsymbol{\rho}), \end{aligned}$$

where S denotes the number of scales used to approximate the long-range interaction. In each of the S steps, the network downsamples the density, performs a convolution with filter \mathbf{F}_s , upsamples the result back to the original mesh size, and sums all the contributions to get the approximate effective potential. Here we assume that n_x is a power of 2 or can be divided by 2 at least $S - 1$ times, and \mathbf{F}_i is the convolution operator at the i th scale with a learnable kernel of size $K = 2n_x/2^{S-1} + 1$ (we keep the filter size odd). The kernel parameters are not shared between the scales. The schematic of the architecture is shown in Fig. 1. In the next section we describe how to find the optimal parameters \mathcal{N}_S .

In the special case with the number of scales $S = 1$ we have a single convolution with a kernel of size $K = 2n_x + 1$, and we recover the exact baseline method $\mathbf{u}^{approx} = \mathbf{F}_0 \boldsymbol{\rho} = \mathbf{u}$ described in the previous section. If $S > 1$, the computations are no longer exact; however, as we show in Sec. III, in such a case we can gain a significant improvement in the performance. Note that we do not use any nonlinear activation function in our neural network \mathcal{N}_S , Eq. (9); hence, it preserves the physically required charge superposition condition $\mathcal{N}_S(a\boldsymbol{\rho} + b\boldsymbol{\rho}') = a\mathcal{N}_S(\boldsymbol{\rho}) + b\mathcal{N}_S(\boldsymbol{\rho}')$.

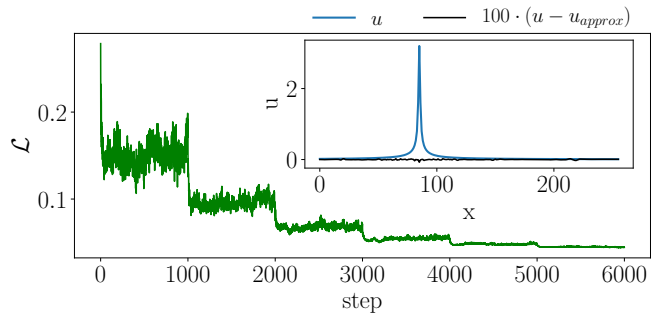


FIG. 2. The loss function across the training iterations. Inset: The potential obtained by the baseline method and the difference between the baseline and approximate result scaled by 100.

3. Finding optimal parameters of \mathcal{N}_S

In order to find the optimal kernel parameters of the neural network \mathcal{N}_S we apply the widely used gradient descent (GD) method²⁷. We use the TensorFlow library³³, which uses the back-propagation method (i.e., chain rule) to compute the analytical value of the gradient of the loss function with respect to the network parameters. In the following we present the loss function and the methodology used to train the network³⁵.

The effective potential can be treated as a superposition of contributions from point like charges at each mesh point. We use this property to define the loss function for our problem. Given a point charge $\rho_p(\mathbf{r}) = \delta(\mathbf{r} - \mathbf{r}_p)$ at position \mathbf{r}_p , we get the exact solution for the integral (8), and the effective potential is given by the kernel function $u_p(\mathbf{r}) = u(\mathbf{r} - \mathbf{r}_p)$. Substituting Dirac's δ for the density in Eq. (8), one obtains

$$u_p(\mathbf{r}_1) = \int d\mathbf{r}_2 u(\mathbf{r}_1 - \mathbf{r}_2) \delta(\mathbf{r}_2 - \mathbf{r}_p) = u(\mathbf{r}_1 - \mathbf{r}_p). \quad (10)$$

To obtain the same result on a discrete grid we use Kronecker's δ instead of Dirac's δ . Using this property, we train the network \mathcal{N}_S to minimize the difference between the exact \mathbf{u}_p discretized potential and the approximated one [Eq. (9)],

$$\mathcal{L} = \frac{1}{n_x} \sum_{p=1}^{n_x} \|\mathcal{N}_S(\boldsymbol{\rho}_p) - \mathbf{u}_p\|^2, \quad (11)$$

where $\|\mathbf{x}\|^2 = \sum_i x_i^2$ is the L_2 norm of vector \mathbf{x} and the sum in the above equation runs over all grid sites. In order to minimize Eq. (11) we use the standard gradient descent using the basic momentum GD optimizer with a decaying learning rate. We decay the learning rate l_r by a factor ϵ every N_{it} gradient updates. The hyperparameters l_r , ϵ , and N_{it} are obtained semi-automatically via a grid search. N_{it} is chosen to be of the order of 2000, and we train the by kernels varying l_r and ϵ in discrete

steps and find their combination that yields the lowest loss function. Note that once the model is trained, it can be reused in many problems assuming that the grid size or the estimated kernel does not change.

Figure 2 shows the loss function throughout the training for the Coulomb interaction potential on a mesh of $n_x = 256$, $S = 4$, $K = 65$, and initial $l_r = 0.003$. The abrupt drop at each multiple of $N_{it} = 1000$ steps occurs when the learning rate is decreased by $\epsilon = 0.5$. The potential evaluated by the integral (7) with the baseline method is shown in the inset of Fig. 2. The difference between the baseline result and the potential obtained with the trained kernels is shown by the black line. The error is scaled by a factor of 100 to be visible, but the approximated potential is close to the baseline. A more quantitative assessment of the accuracy of our method will follow in Sec. III.

4. Isotropic potentials in two dimensions

In the case of isotropic potentials a one-dimensional kernel \mathbf{k}^{1D} array obtained from the method described in the previous section can be projected to two-dimensional (2D) Cartesian coordinates using the projection tensor \mathbf{R} ,

$$k_{ij}^{2D} = \sum_{l=1}^K R_{ijl} k_l^{1D}, \quad i, j \in (1, K); \quad (12)$$

for more information about the details of implementation of \mathbf{R} see Ref. 28. Having computed the two-dimensional kernels \mathbf{k}^{2D} from Eq. (12), we can use them to solve the two-dimensional integrals by replacing all the 1D operators in Eq. (9) by their 2D analog. A similar approach can be used to project the 1D kernel to three dimensions.

Figure 3 shows the best kernels at subsequent scales obtained from the training in Fig. 2. The kernels projected to two dimensions are shown in the bottom row of Fig. 3.

C. Benchmark

First, we determine the computation time using the kernels obtained by our method. Figure 4 shows the average time of the computation for various mesh sizes and numbers of scales, compared to the baseline. The time includes only the computation of the integrals, and not the training. We calculate 100 integrals with ρ and kernels filled with random values. The dashed lines show the average time $T = 2$ and 5 ms for reference. The computational time is shown for the calculation for a single thread and 40 threads, with the neural net implemented in Fortran, and for the calculation on a CPU and GPU for the TensorFlow implementation. We used the GPU GeForce GTX 1080 Ti.

The implementation on a GPU works faster for more scales. On the other hand, the MKL implementation is faster with a smaller number of scales, i.e., for the case that is potentially more precise.

III. APPLICATIONS

A. Two electrons in a harmonic potential

As a first application for the method we present the solution of a problem of two interacting electrons confined in a 2D harmonic potential

$$V(r_i) = \frac{1}{2} m^* \omega^2 r_i^2, \quad (13)$$

with the Coulomb interaction potential

$$u(|\mathbf{r}_i - \mathbf{r}_j|) = \frac{e^2}{4\pi\epsilon_0\epsilon} \frac{1}{|\mathbf{r}_i - \mathbf{r}_j|}. \quad (14)$$

We use the GaAs parameters $m^* = 0.067m_e$ and $\epsilon = 12.4$, where m_e is the electron mass. We solve the problem using the configuration interaction method with the Coulomb integrals calculated by (i) a convolution with an exact $(2n_x + 1) \times (2n_x + 1)$ filter by Fourier transform and (ii) using our method.

This problem can also be solved for two electrons using the semianalytical method described in Ref. 36. In the center-of-mass coordinates the Hamiltonian can be written in the form

$$H = H_{cm} + H_{rel}, \quad (15)$$

where H_{cm} is the center-of-mass Hamiltonian and H_{rel} describes the relative motion of the electrons. H_{cm} is independent of the interaction, and the center-of-mass energy is $E_R = \hbar\omega(n_R^x + n_R^y + 1)$, where n_R^x, n_R^y are the quantum numbers of the center-of-mass energy. Further noting that H_{rel} commutes with the z component of the angular momentum operator, one can write it in the cylindrical coordinates

$$H_{rel,\rho} = -2 \left(\frac{d^2}{d\rho^2} + \frac{1}{\rho} \frac{d}{d\rho} - \frac{M^2}{\rho^2} - \frac{\gamma^2}{4} \rho^2 - \frac{1}{\rho} \right), \quad (16)$$

with $\gamma = \omega/2$, which yields states with a well defined angular momentum quantum number M . Equation (16) is written in donor units with energy in $R_D = \frac{m^* \kappa^2 e^4}{2\hbar^2 \epsilon^2}$, length in units of $a_D = \frac{\hbar^2 \epsilon}{m^* \kappa e^2}$, and $\kappa = 1/4\pi\epsilon_0$. Further, $E = E_{rel} + E_R$. We calculate E_{rel} using the shooting method (see Appendix A). The four lowest levels and their degeneracies d are given in Fig. 5.

For the CI method we take as a basis set $n_{basis}=20$ spin orbitals. We solve the problem on an $n_x \times n_x$ mesh. The results of the calculation with $n_x = 64$ are shown in Fig. 5 together with the results of the shooting method. The results of both methods agree very well. For completeness, we show the results of methods (i) and (ii) for three electrons in Fig. 6.

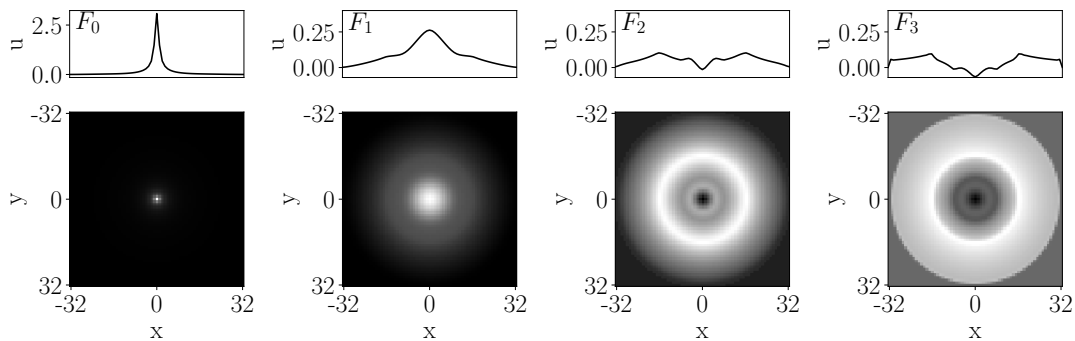


FIG. 3. The kernels obtained from the training in Fig. 2 using Coulomb interaction potential. Top row: the one-dimensional kernels; bottom row: the kernels after the projection to two dimensions [Eq. (12)].

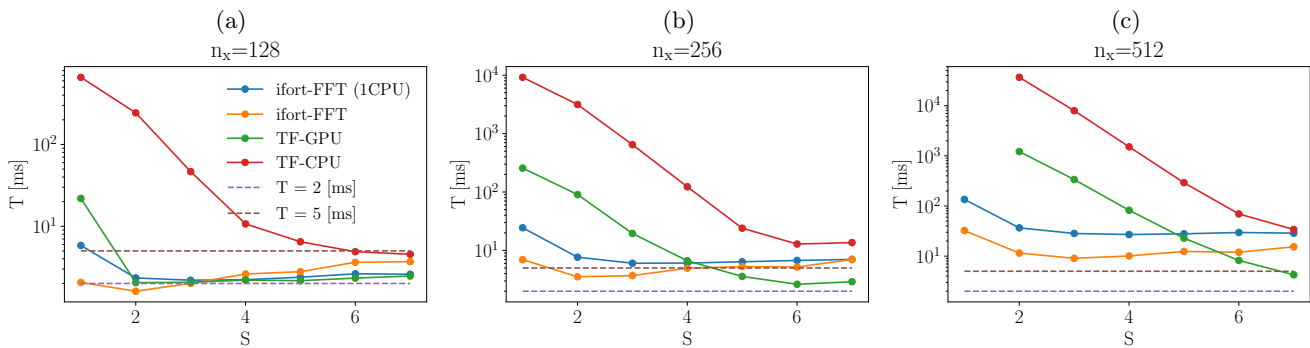


FIG. 4. The calculation time averaged over 100 integrals as a function of the number of scales for mesh size (a) $n_x = 128$, (b) $n_x = 256$ and (c) $n_x = 512$.

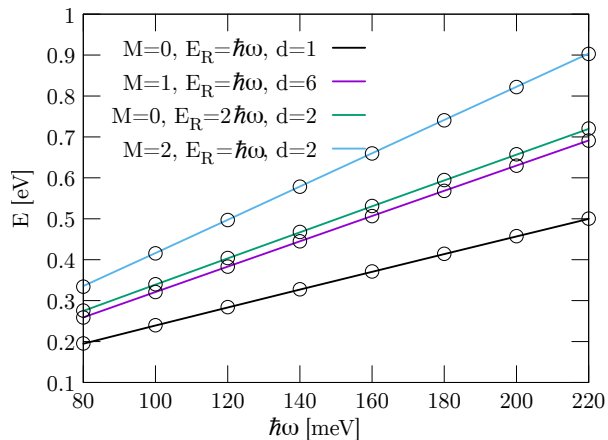


FIG. 5. The four lowest energy levels of two electrons trapped in a harmonic potential as a function of ω . The lines show the solution with the shooting method, and the circles show the solution with the CI method with the Coulomb integrals calculated by our method. M is the angular momentum quantum number, and d denotes the degeneracy of the levels.

We present the performance of our method as n_x is varied from 64 to 512, doubling n_x at each step. The results are obtained for $\hbar\omega = 200$ meV. The hyperparameters

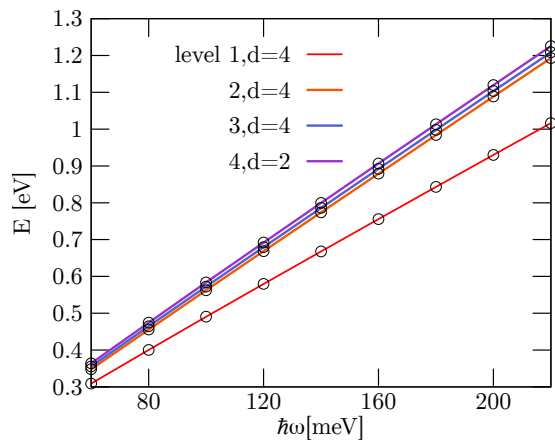


FIG. 6. The four lowest energy levels of three electrons trapped in a harmonic potential as a function of ω . The lines show the numerical solution with method (i), and the circles show that with method (ii). d denotes the degeneracy of the levels.

used for each mesh size are summarized in Table I.

Figures 7(a) and (b) show the difference between the energies obtained with both methods relative to the result of method (i). Method (i), although not exact, will

Interaction potential Eq. (14), 2 dimensions						
n_x	S	K	l_r	ϵ	N_{it}	\mathcal{L}
64	2	65	0.004	0.2	2000	0.0122
128	3	65	0.007	0.4	2000	0.0212
256	4	65	0.003	0.4	2000	0.0271
512	5	65	0.002	0.4	2000	0.0293

TABLE I. Hyperparameters used for training the kernels for Fig. 7 for each mesh of size $n_x \times n_x$ and the obtained loss function \mathcal{L} for the interaction potential (14) in two dimensions.

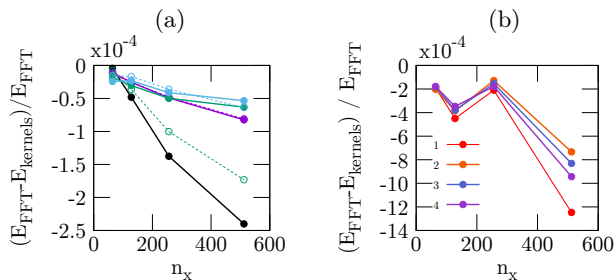


FIG. 7. The difference between energies obtained with both methods relative to the result of method (i) for the respective energy levels shown in the same line color as in Figs. 5 and 6, for (a) two electrons and (b) three electrons.

be more accurate than the approximation of the integral with the sum of scaled convolutions, so we treat it as a reference. Our approach gives energies that are relatively close to the baseline result, and the difference is of the order of 10^{-4} of the baseline energy. For energies on the scale of hundreds of meV (see Fig. 5) the difference is impossible to spot.

We consider the accuracy of the method depending on the number of scales S and size of the kernel K . Figure 8 shows the relative error as a function of the number of scales for a 256×256 mesh. For $S=2, 3, 4, 5$, and 6 , the filter sizes are $K=257, 129, 65, 33$, and 17 , respectively. The parameters used for training the kernels are summarized in Table II.

Interaction potential Eq. (14), 2 dimensions						
n_x	S	K	l_r	ϵ	N_{it}	\mathcal{L}
256	2	257	0.008	0.2	2000	0.0050
256	3	129	0.010	0.2	2000	0.0142
256	4	65	0.005	0.3	2000	0.0267
256	5	33	0.008	0.3	2000	0.0549
256	6	17	0.004	0.3	1800	0.1251

TABLE II. Hyperparameters used for training the kernels for Fig. 8 for a mesh of 256×256 for each K and the obtained loss function \mathcal{L} for the interaction potential (14) in two dimensions.

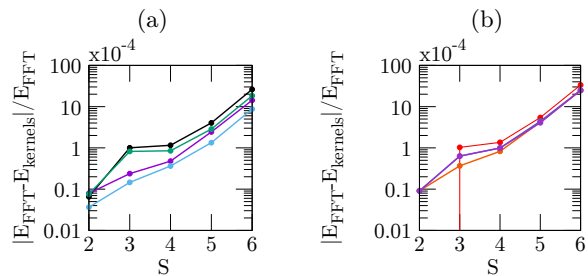


FIG. 8. The difference between energies obtained with both methods relative to the result of method (i) for mesh size $n_x = 256$ as a function of the number of scales. The results are shown for the respective energy levels with the same line color as in Fig. 5. The results are obtained for (a) two electrons and (b) three electrons. The lines are guides to the eye.

As can be expected, for smaller kernels (and a higher number of scales S) the error increases. However, even for the smallest kernel size, the errors do not exceed 4×10^{-3} of the reference energies. The benchmark in Fig. 4 shows that the method tends to be faster for a larger S . Thus choosing the hyperparameters K and S is a trade-off between speedup and accuracy.

B. Effective 1D interaction potential

As the next example of the application of our approach we present the results for the integration of a non-Coulomb interaction potential in 1D systems. We consider a quasi-one-dimensional quantum dot, formed in a semiconductor by strong confinement in two directions³¹. We assume a harmonic oscillator confining potential in the (x, y) direction. Assuming that for a strong lateral confinement the electrons are frozen to the ground harmonic potential state and integrating over the lateral coordinates, one obtains the interaction potential³⁰

$$u(z_{ij}) = (\pi/2)^{\frac{1}{2}} (\kappa/l) \operatorname{erfc}(z_{ij}/2^{\frac{1}{2}}l) \exp(z_{ij}^2/2l^2). \quad (17)$$

Here $z_{ij} = |z_i - z_j|$, and $l = \sqrt{\hbar/m^*\omega}$. The single-electron Hamiltonian (2) is

$$h_i = -\frac{\hbar^2}{2m^*} \frac{d^2}{dz_i^2} + V(z_i), \quad (18)$$

and we assume a 1D infinite well confinement potential in $V(z_i)$.

For a few electrons confined in such quasi-one-dimensional systems, formation of Wigner molecules was observed³¹ for sufficiently long dots. Figures 9(a) and 9(c) show the energies as a function of the length d of the potential well in z for two and three electrons confined in the dot, respectively. The calculations are done

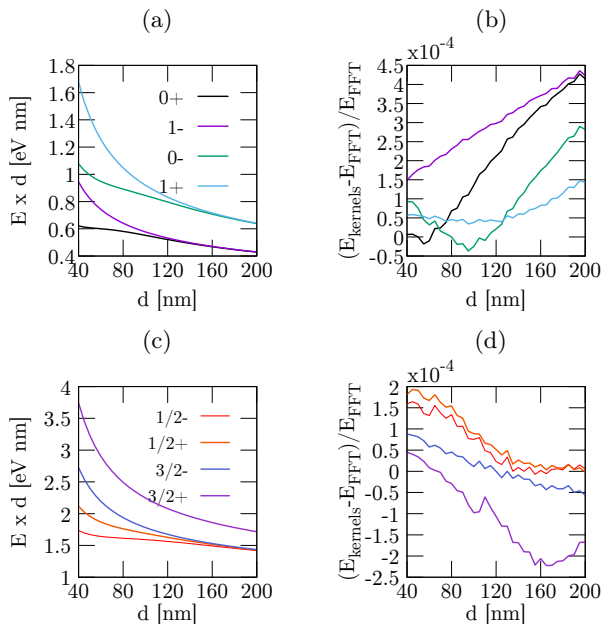


FIG. 9. (a) and (c) The lowest energy levels as a function of the quantum dot length d and (b) and (d) the difference between the results of both methods relative to the method (i) result for the respective energy levels shown in the same line color as in (a) and (c). The results are obtained for two electrons in (a) and (b), and for 3 electrons in (c) and (d).

for mesh $n_x = 256$. For the evaluation of the kernels for our method we used the parameters: $S = 4$, $K = 65$, an initial learning rate of 0.02 decayed by $\epsilon = 0.65$ in ten steps, and $N_{it} = 300$ iterations.

In Figs. 9(b) and 9(d) the relative difference between the results of method (ii) and method (i) is shown. The line colors correspond to the energy levels in Figs. 9(a) and 9(c). The relative error is of the order of 10^{-4} , which allows for a sufficiently good evaluation of the energy levels.

IV. SUMMARY

The calculation of the energy levels of many-body quantum systems is a long-established challenge. Even with the approximate methods including DFT and CI, the computation is time-consuming due to its high complexity, resulting from the need to evaluate a large number of two-electron integrals, among other causes. The aim of this work was to develop a fast and efficient approach to calculate the two-electron integrals for the few-electron calculations. For many problems, it is not crucial to obtain extremely high precision of the integration, and the acceleration of the computation is beneficial provided that the error is much smaller than the order of magnitude of the energies in the system. Our method allows us to significantly reduce the computation time, while maintaining reasonable accuracy. Picking the number of

scales in our method one can choose between higher precision and faster computation. The optimized evaluation of the two-electron integrals can also be used in other methods used on a discrete mesh, e.g., the Hartree-Fock method.

V. ACKNOWLEDGMENT

This research was supported in part by PLGrid Infrastructure.

Appendix A: Shooting method

The problem of two electrons confined in a 2D harmonic potential can be solved semi-analytically³⁶. The relative motion of the electrons is described in cylindrical coordinates by the Hamiltonian (16). We solve it in a discrete mesh using the shooting method. The wavefunction of the relative motion of the electrons $\psi(\rho, \phi) = R(\rho)e^{iM\phi}$, and the mesh is discretized into nodes ρ_i . The relative motion of electrons written in cylindrical coordinates

$$-\frac{1}{2} \left(\frac{d^2}{d\rho^2} + \frac{1}{\rho} \frac{d}{d\rho} - \frac{M^2}{\rho^2} - \frac{\gamma_x^2}{4} \rho^2 - \frac{1}{\rho} \right) R(\rho) = \frac{E}{4} R(\rho), \quad (\text{A1})$$

can be written in the finite-difference approximation with $E' = E/4$,

$$\begin{aligned} & \left(\frac{1}{(\Delta\rho)^2} + \frac{1}{2\rho\Delta\rho} \right) R_{i+1} \\ & = \left(\frac{2}{(\Delta\rho)^2} + \frac{M}{\rho^2} + \frac{\gamma_x^2}{4} \rho^2 + \frac{1}{\rho} - 2E' \right) R_i \\ & \quad + \left(-\frac{1}{(\Delta\rho)^2} + \frac{1}{2\rho\Delta\rho} \right) R_{i-1}, \end{aligned} \quad (\text{A2})$$

where $R_i = R(\rho_i)$ is the wave function at node ρ_i of the finite-difference mesh. In the shooting method we assume the boundary condition $R_0 = 0$ at the left edge of the mesh, and for a given energy we calculate the values of R_i at the nodes of the mesh. We proceed to the right edge of the mesh, and R_{n_x} needs to vanish. This condition is satisfied at discrete values of energy. The problem essentially is to find energies E' at which $R_{n_x} = 0$ in Eq. (A2).

Appendix B: Effectiveness of the method

We consider the effectiveness of the method with respect to the number of electrons and dimensionality. We use the CI method, with n basis states $\phi_k(\mathbf{r})$ from which we form the Slater determinants [Eq. (4)], and the number of the two-electron integrals depends only on the size of the basis n , irrespective of the number of electrons. In our method the calculation of two-electron integrals

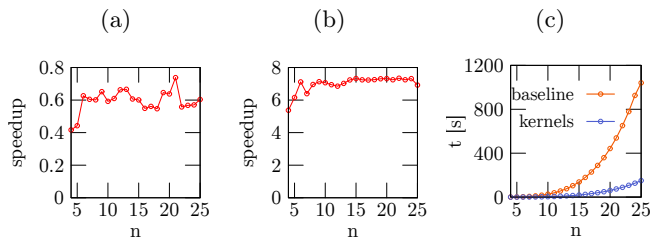


FIG. 10. Speedup of the method as a function of the number of base states n for calculations of two electrons in (a) one dimension and (b) two dimensions and (c) the time of the calculation for the 2D case.

is optimized via ML, thus the speedup depends only on the number of the basis states. In Fig. 10 we present the speedup (the ratio of the time of calculation by our method to the baseline time) as a function of n , obtained for electrons in one dimension [Fig. 10(a)] and two dimensions [Fig. 10(b)] on a mesh with $n_x = 256$, and a kernel with $K = 65$, $S = 4$. In two dimensions the calculation with our method is several times faster than using FFT. In one dimension our method is slightly slower than the baseline because it performs several additional operations (upsampling, downsampling) that in one dimension get less boost in parallelization. Importantly, our method gains more boost for two or more dimensions, and the

results in one dimension are shown for presentation purposes.

Table III shows the total energies and the interaction energies of the two lowest levels calculated for two to four electrons and the error of our method relative to the baseline. The error tends to increase with the number of electrons; however, it does not change linearly, as one would expect. We found that the increase is of the same order as the increase of the interaction energy. The reason is that our method optimizes the evaluation of the interaction integrals; thus, the error will scale in a manner similar to the interaction energy.

N	Level	E_{FFT} (eV)	E_{int} (eV)	$E_{FFT} - E_{kernels}$ (eV)
2	1	0.32727	0.04727	6×10^{-6}
2	2	0.44457	0.16457	3.2×10^{-5}
3	1	0.66788	0.24788	6.1×10^{-5}
3	2	0.773875	0.353875	9.6×10^{-5}
4	1	1.03282	0.47282	1.6×10^{-4}
4	2	1.04097	0.48097	1.8×10^{-4}

TABLE III. Total energy and interaction energy of the lowest levels, and the error of our method relative to the baseline calculated for two, three and four electrons confined in a 2D harmonic potential.

- ¹ Giuseppe Carleo and Matthias Troyer, “Solving the quantum many-body problem with artificial neural networks,” *Science* **355**, 602 (2017).
- ² Giuseppe Carleo, Yusuke Nomura, and Masatoshi Imada, “Constructing exact representations of quantum many-body systems with deep neural networks,” *Nature Communications* **9**, 5322 (2018).
- ³ Bartłomiej Gardas, Marek M. Rams, and Jacek Dziarmaga, “Quantum neural networks to simulate many-body quantum systems,” *Phys. Rev. B* **98**, 184304 (2018).
- ⁴ Zi Cai and Jinguo Liu, “Approximating quantum many-body wave functions using artificial neural networks,” *Phys. Rev. B* **97**, 035116 (2018).
- ⁵ Alberto Fabrizio, Andrea Grisafi, Benjamin Meyer, Michele Ceriotti, and Clemence Corminboeuf, “Electron density learning of non-covalent systems,” *Chem. Sci.* **10**, 9424 (2019).
- ⁶ K. T. Schütt, M. Gastegger, A. Tkatchenko, K.-R. Müller, and R. J. Maurer, “Unifying machine learning and quantum chemistry with a deep neural network for molecular wavefunctions,” *Nat. Commun.* **10**, 5024 (2019).
- ⁷ Andrea Grisafi, Alberto Fabrizio, Benjamin Meyer, David M. Wilkins, Clemence Corminboeuf, and Michele Ceriotti, “Transferable machine-learning model of the electron density,” *ACS Cent. Sci.* **5**, 57 (2019).
- ⁸ Jiequn Han, Linfeng Zhang, and Weinan E, “Solving many-electron Schrödinger equation using deep neural networks,” *J. Comput. Phys.* **399**, 108929 (2019).
- ⁹ Jan Hermann, Zeno Schätzle, and Frank Noé, “Deep neu-

- ral network solution of the electronic Schrödinger equation,” .
- ¹⁰ Jonas B. Rigo and Andrew K. Mitchell, “Machine learning effective models for quantum systems,” *Phys. Rev. B* **101**, 241105(R) (2020).
- ¹¹ Junwei Liu, Yang Qi, Zi Yang Meng, and Liang Fu, “Self-learning Monte Carlo method,” *Phys. Rev. B* **95**, 041101(R) (2017).
- ¹² Yuki Nagai, Huitao Shen, Yang Qi, Junwei Liu, and Liang Fu, “Self-learning Monte Carlo method: Continuous-time algorithm,” *Phys. Rev. B* **96**, 161102(R) (2017).
- ¹³ Huitao Shen, Junwei Liu, and Liang Fu, “Self-learning Monte Carlo with deep neural networks,” *Phys. Rev. B* **97**, 205140 (2018).
- ¹⁴ P. Hohenberg and W. Kohn, “Inhomogeneous electron gas,” *Phys. Rev.* **136**, B864 (1964).
- ¹⁵ Douglas Rayner Hartree and W. Hartree, “Self-consistent field, with exchange, for beryllium,” *Proc. R. Soc. London, Ser A.* **150**, 9 (1935).
- ¹⁶ C. C. J. Roothaan, “Self-consistent field theory for open shells of electronic systems,” *Rev. Mod. Phys.* **32**, 179 (1960).
- ¹⁷ Isaiah Shavitt, “The method of configuration interaction,” in *Methods of Electronic Structure Theory*, edited by Henry F. Schaefer (Springer US, Boston, MA, 1977) p. 189.
- ¹⁸ John A. Pople, Martin Head-Gordon, and Krishnan Raghavachari, “Quadratic configuration interaction. A general technique for determining electron correlation en-

- ergies,” *J. Chem. Phys.* **87**, 5968 (1987).
- ¹⁹ Massimo Rontani, Carlo Cavazzoni, Devis Bellucci, and Guido Goldoni, “Full configuration interaction approach to the few-electron problem in artificial atoms,” *J. Chem. Phys.* **124**, 124102 (2006).
- ²⁰ Irene Puerto Gimenez, Marek Korkusinski, and Pawel Hawrylak, “Linear combination of harmonic orbitals and configuration interaction method for the voltage control of exchange interaction in gated lateral quantum dot networks,” *Phys. Rev. B* **76**, 075336 (2007).
- ²¹ Gregory Beylkin, Christopher Kurcz, and Lucas Monzón, “Fast convolution with the free space Helmholtz Green’s function,” *J. Comput. Phys.* **228**, 2770 (2009).
- ²² Luigi Genovese, Thierry Deutsch, Alexey Neelov, Stefan Goedecker, and Gregory Beylkin, “Efficient solution of Poisson’s equation with free boundary conditions,” *J. Chem. Phys.* **125**, 074105 (2006).
- ²³ Lukas Exl, Norbert J. Mauser, and Yong Zhang, “Accurate and efficient computation of nonlocal potentials based on gaussian-sum approximation,” *J. Comput. Phys.* **327**, 629 (2016).
- ²⁴ S. C. Mukherjee, K. Roy, and N. C. Sil, “Evaluation of the Coulomb integral for scattering problems,” *Phys. Rev. A* **12**, 1719 (1975).
- ²⁵ Michał Lesiuk and Robert Moszynski, “Reexamination of the calculation of two-center, two-electron integrals over Slater-type orbitals. i. Coulomb and hybrid integrals,” *Phys. Rev. E* **90**, 063318 (2014).
- ²⁶ Mieke Peels and Gerald Knizia, “Fast evaluation of two-center integrals over gaussian charge distributions and gaussian orbitals with general interaction kernels,” *Journal of Chemical Theory and Computation* **16**, 2570 (2020).
- ²⁷ Ian Goodfellow, Yoshua Bengio, and Aaron Courville, *Deep Learning* (MIT Press, Cambridge, MA, 2016).
- ²⁸ The source code for the implementation of the proposed method can be found at: <https://github.com/kmkolasinski/approxkernel>.
- ²⁹ Pierluigi Cudazzo, Ilya V. Tokatly, and Angel Rubio, “Dielectric screening in two-dimensional insulators: Implications for excitonic and impurity states in graphane,” *Phys. Rev. B* **84**, 085406 (2011).
- ³⁰ Stanisław Bednarek, Bartłomiej Szafran, Tomasz Chwiej, and Janusz Adamowski, “Effective interaction for charge carriers confined in quasi-one-dimensional nanostructures,” *Phys. Rev. B* **68**, 045328 (2003).
- ³¹ Bartłomiej Szafran, Francois M. Peeters, Stanisław Bednarek, Tomasz Chwiej, and Janusz Adamowski, “Spatial ordering of charge and spin in quasi-one-dimensional Wigner molecules,” *Phys. Rev. B* **70**, 035401 (2004).
- ³² For the Intel[®] MKL documentation we refer to <https://software.intel.com/en-us/mkl-developer-reference-c-convolution-and-correlation>.
- ³³ Martín Abadi, Ashish Agarwal, Paul Barham, Eugene Brevdo, Zhifeng Chen, Craig Citro, Greg S. Corrado, Andy Davis, Jeffrey Dean, Matthieu Devin, Sanjay Ghemawat, Ian Goodfellow, Andrew Harp, Geoffrey Irving, Michael Isard, Yangqing Jia, Rafal Jozefowicz, Lukasz Kaiser, Manjunath Kudlur, Josh Levenberg, Dan Mané, Rajat Monga, Sherry Moore, Derek Murray, Chris Olah, Mike Schuster, Jonathon Shlens, Benoit Steiner, Ilya Sutskever, Kunal Talwar, Paul Tucker, Vincent Vanhoucke, Vijay Vasudevan, Fernanda Viégas, Oriol Vinyals, Pete Warden, Martin Wattenberg, Martin Wicke, Yuan Yu, and Xiaoqiang Zheng, “TensorFlow: Large-scale machine learning on heterogeneous systems,” <http://tensorflow.org>.
- ³⁴ Adam Paszke, Sam Gross, Francisco Massa, Adam Lerer, James Bradbury, Gregory Chanan, Trevor Killeen, Zeming Lin, Natalia Gimelshein, Luca Antiga, Alban Desmaison, Andreas Kopf, Edward Yang, Zachary DeVito, Martin Raison, Alykhan Tejani, Sasank Chilamkurthy, Benoit Steiner, Lu Fang, Junjie Bai, and Soumith Chintala, “Pytorch: An imperative style, high-performance deep learning library,” in *Advances in Neural Information Processing Systems 32*, edited by H. Wallach, H. Larochelle, A. Beygelzimer, F. d’Alché-Buc, E. Fox, and R. Garnett (Curran Associates, 2019) p. 8024.
- ³⁵ The optimization problem of the network is linear, but it is not trivial to reduce it to a system of linear equations $\mathbf{Ax} = \mathbf{b}$; thus, we use the standard approach of training the network that is quick and efficient.
- ³⁶ Bartłomiej Szafran, Janusz Adamowski, and Stanisław Bednarek, “Electron-electron correlation in quantum dots,” *Phys. E* **5**, 185 (1999).